

Water adsorption performance of UiO-66 modified by $MgCl_2$ for heat transformation applications

Jia-Li Liu(刘佳丽), Guo-Dong Fu(付国栋), Ping Wu(吴平), Shang Liu(刘尚), Jin-Guang Yang(杨金光), Shi-Ping Zhang(张师平), Li Wang(王立), Min Xu(许闽), and Xiu-Lan Huai(淮秀兰)

Citation: Chin. Phys. B, 2022, 31 (**11**): 118101. DOI: 10.1088/1674-1056/ac7b1f

What follows is a list of articles you may be interested in

High adsorption and separation performance ofCO_2 over N_2 in azo-based (N=N) pillar[6]arene supramolecular organic frameworks

Yong-Chao Jiang(姜永超), Gui-Xia Li(李桂霞), Gui-Feng Yu(于桂凤), Juan Wang(王娟), Shu-Lai Huang(黄树来), and Guo-Liang Xu(徐国亮)

Chin. Phys. B, 2021, 30 (**11**): 118105. DOI: 10.1088/1674-1056/ac05b5

Adsorption of CO_2 on MgAl layered double hydroxides: Effect of intercalated anion and alkaline etching time

Yan-Yan Feng(冯艳艳), Xiao-Di Niu(牛潇迪), Yong-Hui Xu (徐永辉), and Wen Yang(杨文)

Chin. Phys. B, 2021, 30 (**4**): 048101. DOI: 10.1088/1674-1056/abd750

Influence of an inserted bar on the flow regimes in the hopper

Yi Peng(彭毅), Sheng Zhang(张晟), Mengke Wang(王梦柯), Guanghui Yang(杨光辉), Jiangfeng Wan(万江锋), Liangwen Chen(陈良文), and Lei Yang(杨磊)

Chin. Phys. B, 2021, 30 (**2**): 028101. DOI: 10.1088/1674-1056/abcf40

A numerical study of dynamics in thin hopper flow and granular jet

Meng-Ke Wang(王梦柯), Guang-Hui Yang(杨光辉), Sheng Zhang(张晟), Han-Jie Cai(蔡汉杰), Ping Lin(林平), Liang-Wen Chen(陈良文), Lei Yang(杨磊)

Chin. Phys. B, 2020, 29 (**4**): 048102. DOI: 10.1088/1674-1056/ab7807

Comparison study of GaN films grown on porous andplanar GaN templates

Shan Ding(丁姗), Yue-Wen Li(李悦文), Xiang-Qian Xiu(修向前), Xue-Mei Hua(华雪梅), Zi-Li Xie(谢自力), Tao Tao(陶涛), Peng Chen(陈鹏), Bin Liu(刘斌), Rong Zhang(张荣), You-Dou Zheng(郑有炓)

Chin. Phys. B, 2020, 29 (**3**): 038103. DOI: 10.1088/1674-1056/ab6c48

Water adsorption performance of UiO-66 modified by $MgCl_2$ for heat transformation applications

Jia-Li Liu(刘佳丽)[1], Guo-Dong Fu(付国栋)[1], Ping Wu(吴平)[1,†], Shang Liu(刘尚)[1], Jin-Guang Yang(杨金光)[1], Shi-Ping Zhang(张师平)[1], Li Wang(王立)[2], Min Xu(许闽)[3], and Xiu-Lan Huai(淮秀兰)[3]

[1] *Beijing Key Laboratory for Magneto-Photoelectrical Composite and Interface Science, School of Mathematics and Physics, University of Science and Technology Beijing, Beijing* 100083, *China*

[2] *School of Energy and Environmental Engineering, University of Science and Technology Beijing, Beijing* 100083, *China*

[3] *Institute of Engineering Thermophysics, Chinese Academy of Sciences, Beijing* 100190, *China*

(Received 1 April 2022; revised manuscript received 19 June 2022; accepted manuscript online 22 June 2022)

UiO-66 is a potential material for adsorption heat transformation (AHT) with high specific surface area, and excellent thermal and chemical stability. However, the low water adsorption capacity of UiO-66 in the low relative pressure range ($0 < P/P_0 < 0.3$) limits its application in AHT. We prepare the UiO-66 modified by $MgCl_2$ through using the solvothermal method and impregnation method, and study their water vapor adsorption performances and heat storage capacities. Attributed to the extremely high saturated water uptake and excellent hydrophilicity of $MgCl_2$, the water adsorption performance of UiO-66 is improved, although the introduction of $MgCl_2$ reduces its specific surface area and pore volume. The water adsorption capacity at $P/P_0 = 0.3$ and the saturated water adsorption capacity of the UiO-66 (with $MgCl_2$ content of 0.57 wt%) modified by the solvothermal method are 0.27 g/g and 0.57 g/g at 298 K, respectively, which are 68.8% and 32.6% higher than the counterparts of pure UiO-66, respectively. Comparing with pure UiO-66, the water adsorption capacity of the UiO-66 (with $MgCl_2$ content of 1.02 wt%) modified by the impregnation method is increased by 56.3% and 14.0% at the same pressure, respectively. During 20 water adsorption/desorption cycles, the above two materials show high heat storage densities ($\sim$ 1293 J/g and 1378 J/g). Therein, the UiO-66 modified by the solvothermal method exhibits the excellent cyclic stability. These results suggest that the introduction of an appropriate amount of $MgCl_2$ makes UiO-66 more suitable for AHT applications.

Keywords: adsorption heat transformation, UiO-66, water vapor adsorption, $MgCl_2$

PACS: 81.05.Rm, 81.05.–t, 88.80.–q, 88.05.Sv **DOI:** 10.1088/1674-1056/ac7b1f

1. Introduction

Global heating and refrigeration energy demand continue to rise, resulting in high consumption of fossil fuels and CO_2 emissions. In order to alleviate these environmental issues, people choose to use cleaner energy, such as solar energy and geothermal energy. In recent years, adsorption heat transformation (AHT) has attracted extensive attention. It can effectively utilize solar energy and industrial waste heat as regeneration and driving energy, and realize heating and refrigeration through the adsorption–desorption cycles of working fluid.[1,2] Vapors such as methanol, ethanol, and water can be used as working fluids in the AHT system. Water vapor is widely used because of its environmental friendliness and high evaporation enthalpy of 2500 kJ/kg.[3,4] At present, many porous materials can be used as adsorbents for AHT, including silica gel,[5] activated carbon,[6,7] zeolite,[8] aluminum phosphate,[9,10] and metal–organic framework materials (MOFs).[11–14] In comparison with silica gel, zeolite, and other traditional porous materials, MOFs have much higher specific surface area[15] and pore volume,[16] as well as the characteristic of adjustable pore structure.[17,18] Because of these properties, MOFs have substantial advantages for AHT applications.

UiO-66 is a kind of MOFs that was discovered by Cavka *et al.*[19] in 2008. It is a potential AHT material with high specific surface area and outstanding thermal and chemical stability.[11,12] The saturated water adsorption capacity of UiO-66 reached about 0.36 g/g.[11,20] In most of AHT applications, porous materials needed superior water adsorption performances within a relative humidity range of $0.05 < P/P_0 < 0.32$.[21] However, the water adsorption capacity of UiO-66 reached just 0.1 g/g–0.2 g/g at $P/P_0 = 0.3$,[11,22] which should be improved. The UiO-66 was modified mainly by introducing functional groups[11,23] and metal ions[24–26] to enhance its adsorption performance. For instance, by introducing functional groups $-NH^{3+}Cl^{-}$, the water adsorption capacity of UiO-66 was increased to 0.55 g/g at $P/P_0 = 0.3$ and 0.64 g/g at $P/P_0 = 0.9$.[11] By doping Cr ions, the water adsorption capacity of UiO-66 at the same relative pressure could be increased to 0.28 g/g and 0.69 g/g correspondingly.[24] In recent years, some researchers have attempted to obtain adsorbents with better water adsorption performance by impregnating UiO-66 with the inorganic salt solution. For example, the adsorbents based on UiO-66 were prepared with $CaCl_2$[27] or LiCl[28] as an active component. Their maximum saturated

[†]Corresponding author. E-mail: pingwu@sas.ustb.edu.cn

© 2022 Chinese Physical Society and IOP Publishing Ltd

water adsorption capacities reached 1.93 g/g and 2.15 g/g, respectively. Therein, the water adsorption capacity of the adsorbent with LiCl as the active component could reach 0.59 g/g at $P/P_0 = 0.3$. As stated above, impregnating inorganic salts solution can significantly improve the water adsorption performance of UiO-66, which is superior to introducing functional groups and metal ions. However, the adsorbents prepared by this method contain a quite large quantity of inorganic salts, which are prone to deliquescence and expansion during the adsorption/desorption cycles. Therefore, the methods of improving the cyclic stability of the adsorbents remain to be explored.

$MgCl_2$ is a cheap[29] and clean inorganic salt with excellent hydrophilicity and high water adsorption performance, its saturated water adsorption capacity can reach 1.11 g/g. At 150 °C, the desorption heat of hydrate $MgCl_2{\cdot}6H_2O$ is 2890 J/g,[30] which shows high heat storage capacity. The water adsorption performance and heat storage capacity of $MgCl_2$ are significantly higher than those of UiO-66. Therefore, introducing $MgCl_2$ into UiO-66 may improve these properties of UiO-66. In the present work, different content of $MgCl_2$ is introduced into UiO-66 by the solvothermal method and impregnation method. The structure and properties of the modified UiO-66 are characterized by scanning electron microscopy (SEM), x-ray diffraction (XRD), water vapor adsorption test, *etc*. The results show that the introduction of an appropriate amount of $MgCl_2$ effectively improves the water adsorption performance and heat storage capacity of UiO-66. Therein, the sample prepared by solvothermal method exhibits better water adsorption performance and cyclic stability.

2. Experiment

2.1. Materials

The chemicals for preparing samples were zirconium chloride ($ZrCl_4$, 98.0%) that was bought from Shanghai Merrill Chemical Technology Company, hydrochloric acid (HCl, 36.0%–38.0%) that was bought from Sinopharm Chemical Reagent Company, N, N-dimethylformamide (DMF, $\geq$ 99.5%), and anhydrous methanol (CH_3OH, $\geq$ 99.5%) that were bought from Beijing Tongguang Fine Chemical Company, 1,4-benzene dicarboxylic acid (H_2BDC, 99.0%) and anhydrous magnesium chloride ($MgCl_2$, 99.0%) that were purchased from Beijing Honghu Chemical Products Company. No further purification was carried out.

2.2. Synthesis of samples

Pure UiO-66 was synthesized according to the Shearer *et al*.'s method.[31] 1.89-g $ZrCl_4$ (8.10 mmol) and 2.69-g H_2BDC (16.20 mmol) were dissolved in 49.0 mL of DMF, then 1.5mL of HCl was added dropwise into the solution. After being stirred for 2 h, the solution was poured into a 100.0-mL sealed reactor and kept at 220 °C for 20 h. The product was centrifuged, and the precipitate was washed with DMF and methanol for 2 h sequentially. The product was dried at 80 °C for 8 h, and then at 250 °C for 2 h. The sample was called $1^{\#}$.

Table 1. Experimental conditions and numbered samples.

Sample number	Modification method	Molar ratio of Mg/Zr in the reactants	Concentration of $MgCl_2$ aqueous solution (mol/L)
$1^{\#}$	pure UiO-66	–	–
$2^{\#}$	solvothermal	0.2:1.0	–
$3^{\#}$	solvothermal	0.5:1.0	–
$4^{\#}$	solvothermal	1.0:1.0	–
$5^{\#}$	solvothermal	1.5:1.0	–
$6^{\#}$	wash $3^{\#}$ with deionized water	–	–
$7^{\#}$	impregnation	–	3.0
$8^{\#}$	impregnation	–	4.5
$9^{\#}$	impregnation	–	6.0

The UiO-66 modified by $MgCl_2$ with the solvothermal method was prepared as follows. 49.0-mL DMF was first placed in each of four 100.0-mL conical flasks. Then, 1.89-g $ZrCl_4$ (8.10 mmol) and 2.69-g H_2BDC (16.20 mmol) were dissolved in DMF sequentially, and 1.5-mL HCl was added dropwise into each of the conical flasks. Finally, 0.15-g, 0.39-g, 0.77-g, and 1.16-g $MgCl_2$ (corresponding to 1.62, 4.05, 8.10, and 12.15 mmol, respectively) were added respectively into four conical flasks, and the molar ratios of Mg/Zr were 0.2:1.0, 0.5:1.0, 1.0:1.0, and 1.5:1.0, respectively. After being stirred for 2 h, the solutions in conical flasks were poured into four 100.0-mL sealed reactors and kept at 220 °C for 20 h. The products were centrifuged, and the precipitates were washed with DMF and methanol for 2 h separately. The products were dried at 80 °C for 8 h and then at 250 °C for 2 h. The samples were named $2^{\#}$, $3^{\#}$, $4^{\#}$, and $5^{\#}$ respectively. 0.11-g substance of $3^{\#}$ was washed with deionized water for 24 h, then centrifuged and dried, and the resulting substance was named $6^{\#}$.

The UiO-66 modified by $MgCl_2$ with the impregnation method was prepared as follows. 10.0-mL $MgCl_2$ aqueous so-

lution was prepared in each of three 25.0-mL conical flasks with concentrations of 3.0, 4.5, and 6.0 mol/L, respectively. 0.50-g pure UiO-66 ($1^{\#}$) was added into each of the conical flasks, stirred for 2 h, and then stood for 24 h. The aqueous solution was centrifuged, and the precipitates were washed with 10.0-mL deionized water for 5 min to remove the $MgCl_2$ attached to the outer surface of UiO-66. After being washed, the samples were centrifuged and then dried at 80 °C for 12 h. The obtained samples were named $7^{\#}$, $8^{\#}$, and $9^{\#}$ respectively.

The corresponding experimental conditions of all samples are shown in Table 1.

2.3. Characterizations of samples

Morphology was detected by a field emission scanning electron microscopy (Supra 55, Carl Zeiss, German), and the surfaces of samples were sprayed with gold prior to detection. Crystal structure was characterized by an x-ray diffraction analyzer (D/max 2500X, Rigaku, Japan). Cu $K\alpha$ ray ($\lambda = 1.54056$ Å) (40 kV, 200 mA) was used as the XRD source, and 2θ was scanned in a range of 5°–50° in steps of 0.01°. The angle calibration was conducted by adding a certain amount of silicon into each sample. Using LambdaFTIR-7600 spectrometer, the Fourier transform infrared (FTIR) spectra in a wavelength range of 400 cm^{-1}–2000 cm^{-1} were obtained by the potassium bromide tableting method. Thermal stability was tested by a synchronous thermal analyzer (STA8000, PerkinElmer, USA). The temperature range was 30 °C–800 °C, and the heating rate was 10 °C/min. Nitrogen adsorption isotherms and water vapor adsorption isotherms were obtained by a specific surface aperture analyzer (BSD-PM1/2, BeiShiDe, China), and samples were degassed at 423 K for 10 h prior to the measurement. The specific surface area and pore volume were calculated by the Langmuir method and NLDFT method, respectively. The water adsorption/desorption cycles were tested by a synchronous thermal analyzer (STA8000, PerkinElmer, USA). The water vapor partial pressure was maintained at 2.42 kPa. The adsorption was maintained at 303 K for 2 h, and the desorption was performed at 423 K for 1 h, with 20 cycles. The heating rate and cooling rate were both 10 °C/min.

3. Results and discussion

3.1. Characterizations

The XRD patterns of samples are shown in Fig. 1(a). The XRD peaks of each sample are the same as those of the simulated UiO-66, indicating that we successfully prepared pure UiO-66 with proper crystallization. The addition of $MgCl_2$ into the reactants does not affect the formation of UiO-66, and the structure of UiO-66 immersed in $MgCl_2$ aqueous solution also remains unchanged. There is no characteristic peak of $MgCl_2$ in the XRD pattern of each sample, which is similar to the research result of Sun *et al.*[28] The probable reason is that the pores of UiO-66 are too small to form the crystal diffraction phase of the $MgCl_2$. Comparing with Fig. 2, no obviously large $MgCl_2$ particles are observed on the surface, which excludes the possibility of massive crystallization of $MgCl_2$ on the outer surface of UiO-66. Figure 1(b) shows the FTIR spectra of samples. The peak at 1657 cm^{-1} belongs to the symmetrical stretching vibration of the carboxylic acid groups coordinated with the Zr centers.[32] The peak at 1580 cm^{-1} is caused by the asymmetric stretching of O–C–O in the BDC ligands, the peak at 1506 cm^{-1} represents the typical vibration of C=C in the benzene ring, and the strong peak at 1398 cm^{-1} is related to the O–C–O symmetrical stretching of the carboxylic acid group in the BDC ligand.[33] The samples of UiO-66 modified by the two methods show a similar FTIR spectrum to that of pure UiO-66, and no distinct chemical bond is observed.

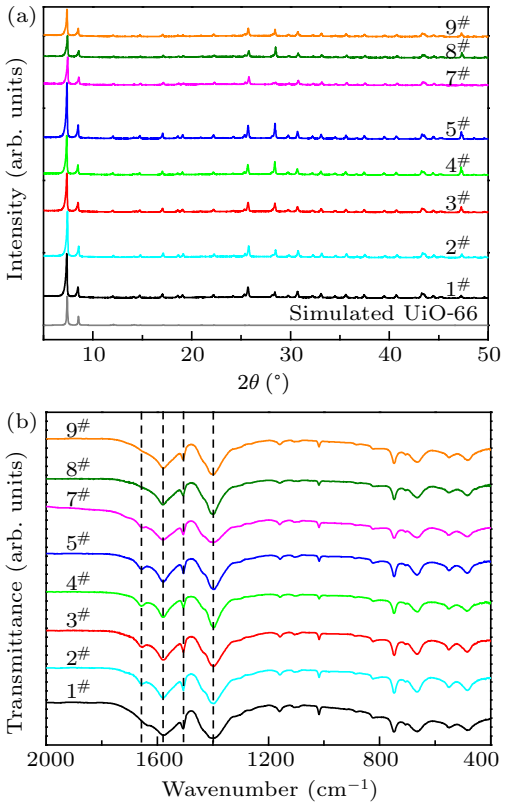


Fig. 1. (a) XRD patterns of simulated UiO-66, pure UiO-66 ($1^{\#}$), and UiO-66 modified by $MgCl_2$ by solvothermal method ($2^{\#}$–$5^{\#}$) and impregnation method ($7^{\#}$–$9^{\#}$), (b) FTIR spectra of pure UiO-66 ($1^{\#}$) and UiO-66 modified by $MgCl_2$ by solvothermal method ($2^{\#}$–$5^{\#}$) and impregnation method ($7^{\#}$–$9^{\#}$).

Figure 2 shows the SEM images and the energy dispersive spectra (EDS) of all samples. Calculated by Nano Measurer software, the morphology of $1^{\#}$ consists of spherical particles with a size of about 285 nm, and the particle sizes of $2^{\#}$–$5^{\#}$ gradually increase. From the SEM images of $2^{\#}$–$5^{\#}$ in Fig. 2, more and more immature UiO-66 particles are tightly agglomerated into large spherical particles, which is similar

to the morphology change of UiO-66 doped by Ce^{+3}.[26] The presence of Mg^{2+} in the reaction solution may inhibit the complete growth of UiO-66 or interfere with the interaction between the Zr metal centers and the organic ligands. According to the EDS spectra, the Mg content in $2^{\#}$–$5^{\#}$ rises gradually, which indicates that the $MgCl_2$ content introduced into UiO-66 increases gradually with the increase of $MgCl_2$ addition in reactants. The particle morphologies of $7^{\#}$–$9^{\#}$ are almost unchanged, which are consistent with the results of XRD, indicating that impregnation does not destroy the structure of UiO-66. The values of Mg content in $7^{\#}$–$9^{\#}$ also rise gradually with the increase of the concentration of $MgCl_2$ aqueous solution. The mass fraction of $MgCl_2$ in sample is calculated according to the EDS spectra, and the result is shown in Table 2. Figure 3 shows the existence of the three elements Zr, Mg, and Cl in samples $3^{\#}$ and $8^{\#}$, and these elements are evenly distributed in the samples. The results show that the solvothermal method and the impregnation method can prepare UiO-66 with good crystallinity, and introduce $MgCl_2$ into UiO-66 successfully.

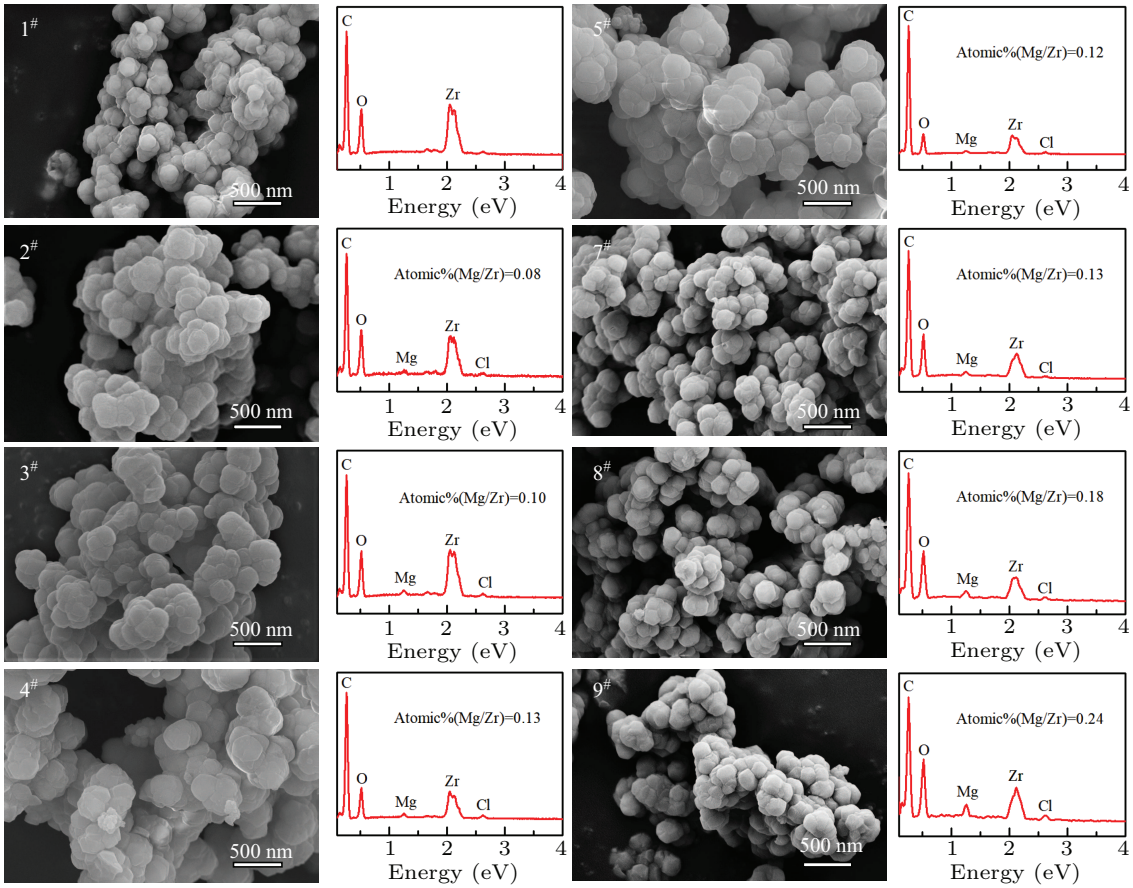


Fig. 2. SEM images and EDS spectra of pure UiO-66 ($1^{\#}$) and UiO-66 modified by $MgCl_2$ through using solvothermal method ($2^{\#}$–$5^{\#}$) and impregnation method ($7^{\#}$–$9^{\#}$).

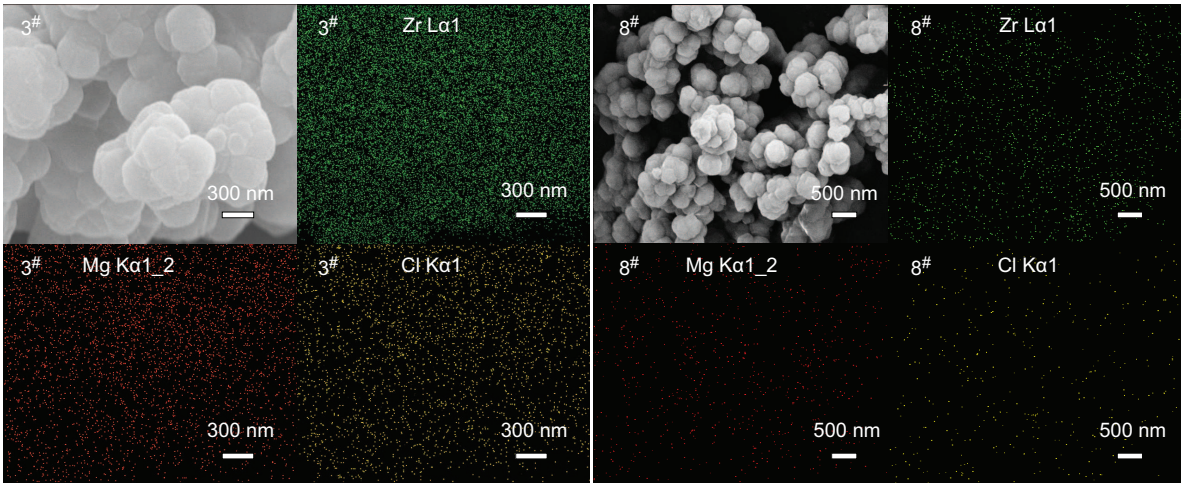


Fig. 3. SEM images and the corresponding EDS element maps of UiO-66 modified by $MgCl_2$ through using solvothermal method ($3^{\#}$) and impregnation method ($8^{\#}$).

Table 2. $MgCl_2$ content in samples.

Samples	Mass fraction of $MgCl_2$ (wt%)
$1^{\#}$	–
$2^{\#}$	0.46
$3^{\#}$	0.57
$4^{\#}$	0.74
$5^{\#}$	0.68
$7^{\#}$	0.74
$8^{\#}$	1.02
$9^{\#}$	1.35

3.2. Thermal stability

The TGA-DTG curves of samples are presented in Fig. 4. The modified samples show the same thermal stability as the pure UiO-66. The weight loss process is mainly divided into three stages, *i.e.*, the loss of physisorption water and residual solvent molecules at temperatures below 200 °C, the dehydroxylation process at temperature between 200 °C and 450 °C, and the complete decomposition of the framework because of the combustion of BDC ligands at a temperature of 450 °C.[34] As shown in Fig. 4(a), the TGA-DTG curves of $2^{\#}$–$5^{\#}$ are consistent with the curve of $1^{\#}$. As $MgCl_2$ content increases, the thermal decomposition temperature gradually moves backward, within a range of 13 °C–34 °C, indicating better thermal stability of the samples. As shown in Fig. 4(b), the weight losses of $7^{\#}$–$9^{\#}$ in the first two stages are all higher than that of $1^{\#}$, which is attributed to the stepwise hydrolysis of $MgCl_2$ doped in samples.[35] Likewise, the thermal decomposition temperature shifts back, and it ranges from 16 °C to 26 °C.

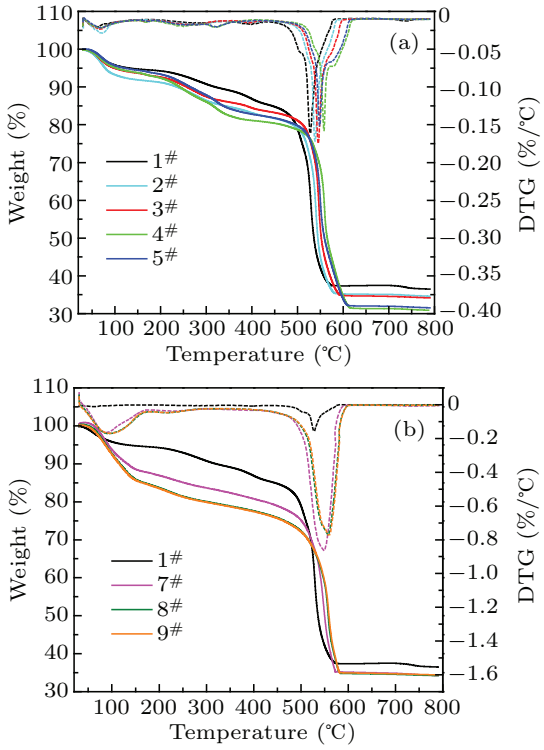


Fig. 4. Thermogravimetric analysis (TGA, solid lines) and derivative thermogravimetry analysis (DTG, dotted lines) curves of pure UiO-66 ($1^{\#}$) and modified UiO-66 by (a) solvothermal method ($2^{\#}$–$5^{\#}$) and (b) impregnation method ($7^{\#}$–$9^{\#}$).

3.3. Porosity characteristics

Figure 5 shows the nitrogen adsorption isotherms of samples at 77 K. The samples show the typical I-type isotherm distributions. In the extremely narrow relative pressure range of $0 < P/P_0 < 0.02$, the nitrogen adsorption capacities of samples increase rapidly. At this phase, the enhanced interaction between adsorbent and adsorbate in the micropores results in the micropore filling phenomenon.[36] After a certain relative pressure is reached, the nitrogen adsorption capacity gradually reaches the limit value. According to Table 3, the BET specific surface area and pore volume of $2^{\#}$–$5^{\#}$ decrease gradually with the increase of $MgCl_2$ content. The specific surface area and pore volume of $6^{\#}$ are similar to those of $1^{\#}$, indicating that the introduction of $MgCl_2$ into UiO-66 does not affect the formation of its pore structure. With the increase of the concentration of $MgCl_2$ solution, the BET specific surface areas and pore volumes of $7^{\#}$–$9^{\#}$ decrease gradually. In conjunction with Mg content changes shown in the EDS energy spectra (Fig. 2), we can infer that more $MgCl_2$ is filled into the pores of UiO-66 as the concentration of $MgCl_2$ solution increases, thus reducing its specific surface area and pore volume.

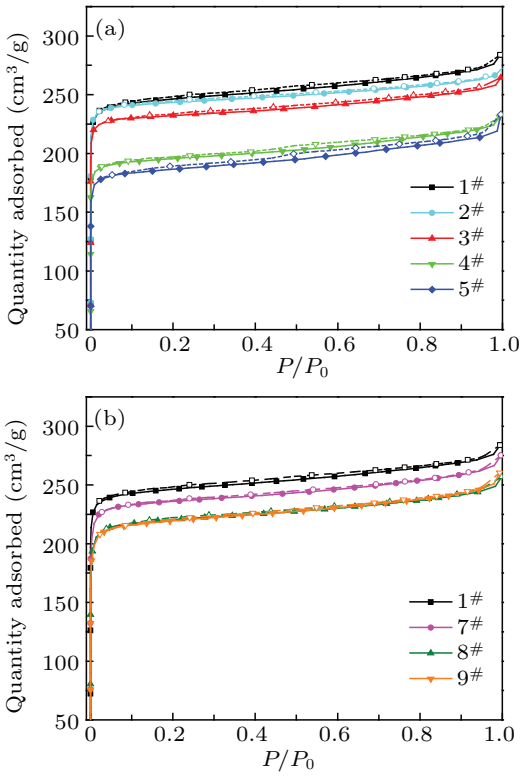


Fig. 5. Nitrogen sorption isotherms of pure UiO-66 ($1^{\#}$) and modified UiO-66 by (a) solvothermal method ($2^{\#}$–$5^{\#}$) and (b) impregnation method ($7^{\#}$–$9^{\#}$) at 77 K, with solid symbols representing adsorption results, and empty symbols denoting desorption results.

Table 3. Porosity characteristics of samples.

Samples	BET surface area (m^2/g)	Langmuir surface area (m^2/g)	$V_{micropore}$ (cm^3/g)	$V_{totalpore}$ (cm^3/g)
1#	742	1092	0.38	0.43
2#	722	1077	0.38	0.41
3#	705	1028	0.36	0.40
4#	582	873	0.30	0.35
5#	570	829	0.29	0.34
6#	762	1137	0.40	0.44
7#	701	1046	0.37	0.41
8#	672	976	0.34	0.38
9#	664	978	0.34	0.39

3.4. Adsorption properties

The water adsorption capacity of UiO-66 at low water pressure ($0 < P/P_0 < 0.3$) is a key characteristic for its application in AHT. The static volumetric method is used to test the water vapor adsorption performances of samples. The water adsorptions of samples conform to the ideal adsorption equilibrium. By changing the relative pressure of water vapor in the sample chamber, the water adsorption capabilities of samples under different relative pressures are measured to obtain the adsorption isotherms (as shown in Fig. 6). The change of water vapor pressure in the sample chamber before and after adsorption (ΔP) are measured by the high-precision pressure sensor. According to the state equation of ideal gas, the molar quantity of the adsorbed water (Δn) can be calculated from the following equation:

$$\Delta n = \frac{\Delta PV}{RT}, \tag{1}$$

where V is the volume of the sample chamber, T is the temperature, and R is the molar gas constant. The water adsorption capacity of the unit mass sample (q_{H_2O}) can be obtained from the following equation:

$$q_{H_2O} = \frac{M_{H_2O} \cdot \Delta n}{m_{sample}}, \tag{2}$$

where M_{H_2O} is the molar mass of water, and m_{sample} is the mass of sample.

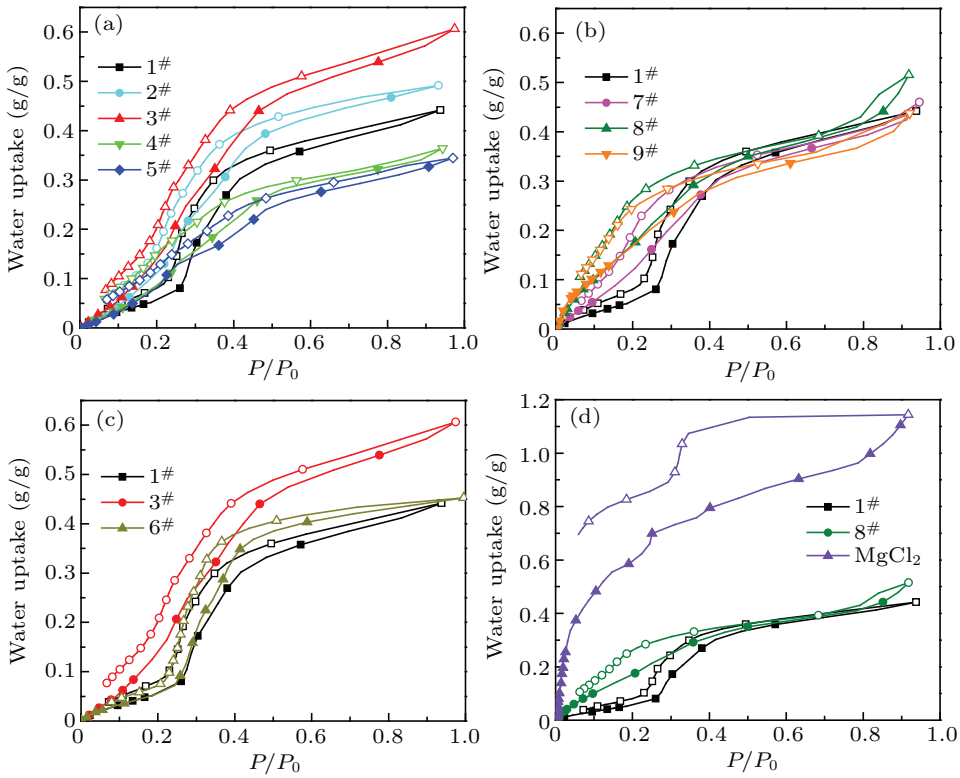


Fig. 6. Water adsorption isotherms of pure UiO-66 (1#), modified UiO-66 by (a) solvothermal method (2#–5#) and (b) impregnation method (7#–9#), (c) 6#, and (d) $MgCl_2$ at 298 K, with solid symbols representing adsorption and empty symbols denoting desorption.

We measure the water vapor adsorption isotherms of pure UiO-66, pure $MgCl_2$, and samples prepared by the two methods to evaluate their water adsorption performances. The adsorption of UiO-66 on the water is physical adsorption. As shown in Fig. 6(a), the isotherm of UiO-66 is the V-type isotherm. At low relative pressure, the adsorption occurs first at the hydrophilic sites where the interaction with water molecules is strong,[37,38] thus the water adsorption capacity increases slowly. At $P/P_0 = 0.3$, the water adsorption capacity of UiO-66 is only 0.16 g/g. With the further increase of water pressure, the adsorbed water molecules continue to adsorb other molecules through the interaction between hydrogen bonds to form clusters for pore filling.[36] In this phase, the water adsorption capacity increases sharply. The water adsorption capacity of UiO-66 at $P/P_0 = 0.9$ reaches 0.43 g/g. Unlike UiO-66, the adsorption of $MgCl_2$ on the water is chemical ad-

sorption. $MgCl_2$ can adsorb a large amount of water even at low water pressure. With the increase of water pressure, anhydrous $MgCl_2$ absorbs water continuously until $MgCl_2{\cdot}6H_2O$ is formed. According to Fig. 6(d) and Table 4, the water adsorption capacity of $MgCl_2$ is 0.73 g/g at $P/P_0 = 0.3$ and 1.11 g/g at $P/P_0 = 0.9$, which is much higher than that of pure UiO-66.

As shown in Fig. 6(a), with the increase of $MgCl_2$ content, the water adsorption capacity of sample first increases ($2^{\#}$ and $3^{\#}$), and then decreases ($4^{\#}$ and $5^{\#}$) at 298 K. Among them, sample $3^{\#}$ has the best water adsorption performance. The water adsorption capacity of $3^{\#}$ at $P/P_0 = 0.3$ is 68.8% and $P/P_0 = 0.9$ is 32.6% higher than that of pure UiO-66, respectively. It is concluded that the introduction of an appropriate amount of $MgCl_2$ is conducive to improving the water adsorption capacity of UiO-66, especially at low relative pressure. The α value in Table 4 is a parameter for evaluating the hydrophilicity of adsorbents. The smaller the α value, the better the hydrophilicity of adsorbent is.[39] The α value of $3^{\#}$ is lower than that of pure UiO-66, indicating that $3^{\#}$ has better hydrophilicity. The water vapor adsorption isotherms of $6^{\#}$ and UiO-66 almost coincide (see Fig. 6(c)), which further indicates that the significant improvement of the water adsorption capacity of $3^{\#}$ is mainly attributed to the $MgCl_2$ in pores. With the increase of $MgCl_2$ content, the specific surface area and pore volume of $4^{\#}$ and $5^{\#}$ decrease significantly (Table 3), thus reducing their water adsorption performance. As can be seen, the total water adsorption capacity of the UiO-66 modified by $MgCl_2$ is determined jointly by $MgCl_2$ and UiO-66. In the modified samples, introducing $MgCl_2$ into the pores of UiO-66 reduces their specific surface areas and pore volumes, whereas the water adsorption capacity of $MgCl_2$ is much higher than that of the same amount of UiO-66. Therefore, after introducing an appropriate amount of $MgCl_2$, the total water adsorption capacity of the sample is still effectively improved.

Table 4. Water uptake parameters of samples.The corresponding P/P_0 value is α when the water adsorption capacity $q = 0.5\ q_{max}$ (q_{max} is the amount of water adsorbed at $P/P_0 = 0.9$).

Samples	Adsorbed water at $P/P_0 = 0.3$ (g/g)	Adsorbed water at $P/P_0 = 0.9$ (g/g)	α
$1^{\#}$	0.16	0.43	0.34
$2^{\#}$	0.23	0.49	0.31
$3^{\#}$	0.27	0.57	0.32
$4^{\#}$	0.16	0.35	0.33
$5^{\#}$	0.15	0.33	0.35
$6^{\#}$	0.18	0.44	0.32
$7^{\#}$	0.21	0.42	0.30
$8^{\#}$	0.25	0.49	0.30
$9^{\#}$	0.23	0.42	0.26

According to Fig. 6(b), the water adsorption capacity of $7^{\#}$, $8^{\#}$, and $9^{\#}$ at $P/P_0 = 0.3$ increases by 31.3%, 56.3%, and 43.8%, respectively, compared with that of UiO-66. The α values of the samples decrease, indicating these samples have better hydrophilicity. Inorganic salt filling reduces the specific surface area and pore volume of UiO-66. Therefore, excessive inorganic salt will reduce the saturated water adsorption capacity of the sample. For example, although $9^{\#}$ has a higher $MgCl_2$ content than $8^{\#}$ (Table 2), its saturated water adsorption capacity is lower. As shown in Fig. 6(d), the water vapor adsorption capacity of $8^{\#}$ is between the counterparts of pure $MgCl_2$ and pure UiO-66. The increase of water adsorption capacity of $8^{\#}$ can be divided into two stages. In the range of $0 < P/P_0 < 0.3$, the water adsorption behavior of $8^{\#}$ is similar to that of $MgCl_2$. The increase in water adsorption capacity mainly comes from the combination of $MgCl_2$ and water. In the range of $0.3 < P/P_0 < 0.9$, the water adsorption behavior of $8^{\#}$ is similar to that of UiO-66, and the increase is mainly attributed to the physical adsorption of water by UiO-66.

3.5. Adsorption cyclic stability

Since the water adsorption performances of $3^{\#}$ and $8^{\#}$ are improved most remarkably, their cyclic stability is tested to further confirm the applicability in the AHT. As shown in Fig. 7, the water adsorption capacity of $3^{\#}$ and $8^{\#}$ in the first cycle is 0.27 g/g and 0.34 g/g, respectively. Then, the water adsorption capacity after 20 cycles is 0.30 g/g and 0.29 g/g. The water adsorption capacity of $3^{\#}$ even slightly increases during circulation. This increase is attributed to the activation and cleaning of pores that may remove the excess hydrophobic sites such as the residual H_2BDC in the repeated adsorption/desorption process.[37] Sample $3^{\#}$ exhibits high stability in the water adsorption/desorption cycles. The water adsorption capacity of $8^{\#}$ decreases with the increase of cycle times, but it tends to be stable after the twelfth cycle. In the process of water adsorption, $MgCl_2$ doped in $8^{\#}$ forms $MgCl_2$ aqueous solution in the pores of UiO-66. The aqueous solution becomes more and more diluted. Once the volume of the solution is larger than the pore volume, the solution will leak out from the pores.[40] During multiple cycles, some leaked $MgCl_2$ may agglomerate. The decrease in the water adsorption capacity of agglomerated $MgCl_2$ leads the water adsorption capacity of $8^{\#}$ to decrease.

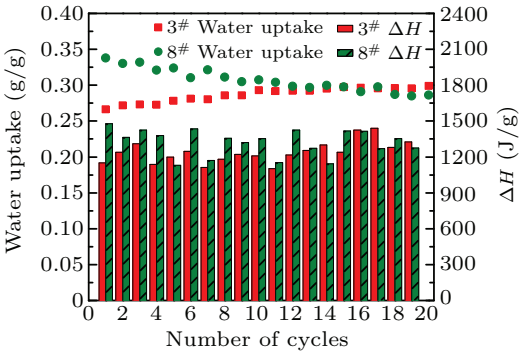


Fig. 7. Water adsorption/desorption cycling performance of UiO-66 modified by solvothermal method ($3^{\#}$) and impregnation method ($8^{\#}$) at 303 K for adsorption and at 423 K for desorption.

The changes in water adsorption capacity and specific surface area of $3^{\#}$ and $8^{\#}$ during circulation are shown in Ta-

ble 5.

Table 5. Influence of cycling on the UiO-66 modified by $MgCl_2$ by solvothermal method ($3^{\#}$) and impregnation method ($8^{\#}$).

Samples	Δwater load (10 cycles) (%)	Δwater load (20 cycles) (%)	ΔS_{BET} (20 cycles) (%)
$3^{\#}$	+7.4	+11.1	–5.1
$8^{\#}$	–8.8	–14.7	–25.0

The cyclic stability of $3^{\#}$ is superior to that of $8^{\#}$. According to the mass of sample and the peak area of the DSC curve, the heat storage density of $3^{\#}$ is 1293 J/g and density of $8^{\#}$ is 1378 J/g. These heat storage densities are higher than those of other porous materials combined with $MgCl_2$, such as graphene (∼ 890 J/g)[41] and Na–Y zeolite (∼ 1173 J/g)[30]

4. Conclusions

The AHT materials of UiO-66 modified by $MgCl_2$ are prepared by the solvothermal method and impregnation method. The modified UiO-66 has high crystallinity, and $MgCl_2$ is evenly distributed in UiO-66, which indicates that the introduction of $MgCl_2$ does not damage the structure of UiO-66. Comparing with pure UiO-66, the thermal decomposition temperature of the modified UiO-66 increases by 13 °C–34 °C, indicating that the thermal stability is enhanced. The specific surface area and pore volume of UiO-66 decrease with the increase of $MgCl_2$ content. Nevertheless, owing to the extremely high saturated water uptake and excellent hydrophilicity of $MgCl_2$, the water adsorption capacity at $P/P_0 = 0.3$ and $P/P_0 = 0.9$ of the UiO-66 (with $MgCl_2$ content of 0.57 wt%) modified by the solvothermal method rise to 0.25 g/g and 0.49 g/g at 298 K, which are 68.8% and 32.6% higher than the counterparts of pure UiO-66. At the same relative pressure, the water adsorption capacity of the UiO-66 (with $MgCl_2$ content of 1.02 wt%) modified by the impregnation method is increased by 56.3% and 14.0%, respectively. During 20 cycles of water adsorption/desorption, the heat storage densities of the two samples mentioned above are 1293 J/g and 1378 J/g, respectively, which are higher than those of $MgCl_2$ combined with graphene (∼ 890 J/g) and Na–Y zeolite (∼ 1173 J/g). Furthermore, the water load of the UiO-66 (with $MgCl_2$ content of 0.57 wt%) modified by the solvothermal method does not decrease after 20 cycles, showing better cyclic stability. In conclusion, the introduction of an appropriate amount of $MgCl_2$ is an effective method of improving the water adsorption performance and heat storage capacity of UiO-66, making it more suitable for AHT.

Acknowledgement

Project supported by the National Natural Science Foundation of China (Grant No. 51836009).

References

[1] Wongsuwan W, Kumar S, Neveu P and Meunier F 2001 *Appl. Therm. Eng.* **21** 1489
[2] Wu W, Zhang X L, Li X T, Shi W X and Wang B L 2012 *Appl. Therm. Eng.* **48** 349
[3] Freni A, Maggio G, Sapienza A, Frazzica A, Restuccia G and Vasta S 2016 *Appl. Therm. Eng.* **104** 85
[4] Jeremias F, Fröhlich D, Janiak C and Henninger S K 2014 *New J. Chem.* **38** 1846
[5] Ng K C, Chua H T, Chung C Y, Loke C H, Kashiwagi T, Akisawa A and Saha B B 2001 *Appl. Therm. Eng.* **21** 1631
[6] Kawano T, Kubota M, Onyango M S, Watanabe F and Matsuda H 2008 *Appl. Therm. Eng.* **28** 865
[7] Kubota M, Ito T, Watanabe F and Matsuda H 2011 *Appl. Therm. Eng.* **31** 1495
[8] Myat A, Kim Choon N, Thu K and Kim Y D 2013 *Appl. Energy* **102** 582
[9] Ristić A, Logar N Z, Henninger S K and Kaučič V 2012 *Adv. Funct. Mater.* **22** 1952
[10] Varlec J, Krajnc A, Mazaj M, Ristić A, Vanatalu K, Oss A, Samoson A, Kaučič V and Mali G 2016 *New J. Chem.* **40** 4178
[11] An H J, Sarker M, Yoo D K and Jhung S H 2019 *Chem. Eng. J.* **373** 1064
[12] Han B and Chakraborty A 2020 *Energy Convers. Manage.* **213** 112825
[13] Wang Q, Tang S L, Tian S, Wei X J and Peng T F 2019 *J. Nanomater.* **2019** 1
[14] Liu S, Wu P, Zhang S P, Fu G D, Yan D, Han X L, Huai X L and Xu M 2021 *Z. Anorg. Allg. Chem.* **647** 1
[15] Farha O K, Eryazici I, Jeong N C, Hauser B G, Wilmer C E, Sarjeant A A, Snurr R Q, Nguyen S T, Yazaydin A O and Hupp J T 2012 *J. Am. Chem. Soc.* **134** 15016
[16] Saha D and Deng S 2010 *Tsinghua Science and Technology* **15** 363
[17] Kim M, Cahill J F, Su Y, Prather K A and Cohen S M 2012 *Chem. Sci.* **3** 126
[18] Yang Q, Wiersum A D, Llewellyn P L, Guillerm V, Serre C and Maurin G 2011 *Chem. Commun. (Camb)* **47** 9603
[19] Cavka J H, Jakobsen S, Olsbye U, Guillou N, Lamberti C, Bordiga S and Lillerud K P 2008 *J. Am. Chem. Soc.* **130** 13850
[20] Henninger S K, Jeremias F, Kummer H and Janiak C 2011 *Eur. J. Inorg. Chem.* **2012** 2625
[21] Zheng X, Ma Q L, Tan J M and Yu B 2021 *Ind. Eng. Chem. Res.* **60** 4727
[22] Makhanya N, Oboirien B, Ren J W, Musyoka N and Sciacovelli A 2021 *J. Energy Storage* **34** 102179
[23] Cmarik G E, Kim M, Cohen S M and Walton K S 2012 *Langmuir* **28** 15606
[24] Fu G D, Wu P, Yang J G, Zhang S P and Huai X L 2022 *Microporous Mesoporous Mater.* **331** 111642
[25] Lau C H, Babarao R and Hill M R 2013 *Chem. Commun. (Camb)* **49** 3634
[26] Ebrahim A M and Bandosz T J 2013 *ACS Appl. Mater. Inter.* **5** 10565
[27] Garzón-Tovar L, Pérez-Carvajal J, Imaz I and Maspoch D 2017 *Adv. Funct. Mater.* **27** 1606424
[28] Sun Y Y, Spieß A, Jansen C, Nuhnen A, Gökpinar S, Wiedey R, Ernst S J and Janiak C 2020 *J. Mater. Chem. A* **8** 13364
[29] Donkers P A J, Sögütoglu L C, Huinink H P, Fischer H R and Adan O C G 2017 *Appl. Energy* **199** 45
[30] Whiting G T, Grondin D, Stosic D, Bennici S and Auroux A 2014 *Sol. Energy Mater. Sol. Cells* **128** 289
[31] Shearer G C, Chavan S, Ethiraj J, Vitillo J G, Svelle S, Olsbye U, Lamberti C, Bordiga S and Lillerud K P 2014 *Chem. Mater.* **26** 4068
[32] Hoa L T, Nhi L T T, Son L V T, Linh N L M, Hai H V M and Khieu D Q 2021 *J. Nanomater.* **2021** 1
[33] Cao Y, Zhao Y X, Lv Z J, Song F J and Zhong Q 2015 *J. Ind. Eng. Chem.* **27** 102
[34] Han Y T, Liu M, Li K Y, Sun Q, Zhang W S, Song C S, Zhang G L, Conrad Zhang Z and Guo X W 2017 *Inorg. Chem. Front.* **4** 1870
[35] Huang Q Z, Lu G M, Wang J and Yu J G 2011 *J. Anal. Appl. Pyrolysis* **91** 159
[36] Thommes M, Kaneko K, Neimark A V, Olivier J P, Rodriguez-Reinoso F, Rouquerol J and Sing K S W 2015 *Pure Appl. Chem.* **87** 1051
[37] Jeremias F, Khutia A, Henninger S K and Janiak C 2012 *J. Mater. Chem.* **22** 10148
[38] Küsgens P, Zgaverdea A, Fritz H G, Siegle S and Kaskel S 2010 *J. Am. Ceram. Soc.* **93** 2476
[39] Canivet J, Bonnefoy J, Daniel C, Legrand A, Coasne B and Farrusseng D 2014 *New J. Chem.* **38** 3102
[40] Glaznev I, Ponomarenko I, Kirik S and Aristov Y 2011 *Int. J. Refrig.* **34** 1244
[41] Ait Ousaleh H, Sair S, Mansouri S, Abboud Y, Faik A and El Bouari A 2020 *Sol. Energy Mater. Sol. Cells* **215** 110601